Journal of Sound and Vibration (2000) **232**(2), 405–430
doi:10.1006/jsvi.1999.2747, available online at http://www.idealibrary.com on IDEAL®

NUMERICAL SOLUTION OF THE STATIONARY FPK EQUATION USING SHANNON WAVELETS

S. McWilliam, D. J. Knappett and C. H. J. Fox

School of Mechanical, Materials, Manufacturing Engineering and Management, Division of Mechanical Engineering, University of Nottingham, Nottingham, NG7 2RD, England

(*Received* 24 *May* 1999, *and in final form* 7 *October* 1999)

The Fokker–Planck–Kolmogorov (FPK) equation governs the probability density function (p.d.f.) of the dynamic response of a particular class of linear or non-linear system to random excitation. This paper proposes a numerical method for calculating the stationary solution of the FPK equation, which is based upon the weighted residual approach using Shannon wavelets as shape functions. The method is developed here for an n-dimensional system and its relationship with the distributed approximating functional (DAF) approach is investigated. For the purposes of validation, numerical results obtained using the proposed method are compared with available exact solutions and numerical solutions for some non-linear oscillators. For the systems considered excellent results over the main body and tails of the marginal distributions are obtained. The accuracy and efficiency of the method are investigated in comparison to the finite element method (FEM).

1. INTRODUCTION

There exist many situations in engineering for which the excitation experienced by engineering structures is random. Some examples of this are the wave and wind loading of offshore structures and the seismic excitation of building structures. In the design of these structures it is vital that the maximum stresses and fatigue life can be predicted so that reliability of the structures can be established. In most cases, a probabilistic analysis is used in which the statistical properties of the response are characterized. For those situations when the system considered behaves linearly and the excitation is Gaussian, the response statistics may be evaluated easily [1]. However, given that non-linearites are present to some extent in most practical engineering structures, it is necessary to take these influences into account when designing structures, since they can have a significant influence on the response statistics of the system. This is particularly the case at the so-called "tails" of the response distribution, which correspond to the larger responses of the structure and give an indication of the probability of failure of the structure.

The Fokker–Planck–Kolmogorov (FPK) equation governs the probability density function (p.d.f) of the response of a particular class of dynamical system to random excitation. This class of system is applicable to systems for which the response is a Markov process and includes linear and non-linear systems subjected to white-noise excitation. For other systems, a FPK equation can be developed provided that the response is a higher order Markov process. Much research effort has been directed at determining exact analytic solutions to the FPK equation [2]. However, limited success in this area has led researchers to develop approximate solution procedures, such as "stochastic averaging" (see, e.g.,

0022-460X/00/170405 + 26 $35.00/0

reference [3]) and numerical techniques [4–15]. It is this final class of solution that is considered in the present work.

Various numerical methods have been used to solve the FPK equation. A recent detailed review of the techniques applied is given by Dunne and Ghanbari [9]. The most commonly used methods include the weighted residual method (WRM) [4, 5], the finite element method (FEM) [6–10], and the path integral method (PIM) [11–13]. A detailed comparison of the FEM and WRM as applied to the stationary solution of the FPK equation has been carried out recently by Dunne and Ghanbari [9]. Based upon computational efficiency in terms of both CPU storage space and time, they concluded that the FEM developed by Langley [6] was more favourable than the WRM. In addition, much effort has been directed at using parallel processing to solve the transient FPK equation using the FEM (see, e.g., [8, 10]). The PIM [11–13] uses the Chapman–Kolmogorov equation to map the evolution in time of the (conditional) p.d.f from a specified initial state. Thus, the PIM solution is well suited to obtaining transient non-stationary probabilities, and probabilities of first-passage failures. After a sufficiently large number of time increments, the p.d.f. converges to a stationary solution. The main advantage of the PIM is that it yields p.d.f.'s that are non-negative, enabling high-accuracy solutions to be obtained at the tails. Recently, Yu *et al.* [13] combined the PIM with a Gauss–Legendre scheme and obtained excellent results for a Duffing oscillator down to p.d.f. values of 10^{-10}. The disadvantage of the PIM is that the transitional p.d.f., which maps the p.d.f. at one time step to the next, is approximated to be *locally* Gaussian and as a result of this it is only accurate to the order of $\mathrm{d}t^2$. For non-Gaussian systems, this time increment $\mathrm{d}t$ must be very small. Consequently, a large number of iterations are usually required for the solution procedure to converge to the stationary solution. Naess and Johnsen [11] have suggested a formula as a guide to the maximum value of $\mathrm{d}t$, but the formula is not suitable for all systems.

Recently, a new numerical method for solving certain types of partial differential equation has been developed by Kouri and co-workers [16–20]. This method is based upon the representation of the unknown response function as a convolution integral in terms of the Dirac delta function. By discretizing this integral an approximation to the function is obtained in terms of its "nodal" values. Provided that an appropriate representation of the Dirac delta function is used, the expression can be differentiated to obtain the derivatives of the function in terms of the nodal values. This so-called DAF approach has been shown to yield highly accurate estimates of the function and its derivatives in terms of its nodal values and provides a simple basis for solving partial differential equations. It has been applied to a variety of problems in physics and has been shown to be both efficient and accurate. To date, this technique has been applied to Burger's equation [18] and Schrödinger's [19] equation, as well as a first order non-linear transient FPK equation [17].

This paper presents a novel numerical method for calculating the stationary solution of the FPK equation. The proposed method is based upon using the weighted residual approach with Shannon wavelets as shape functions. The method is developed for an n-dimensional system and its relationship with the DAF approach is investigated. More specifically, it is shown that the proposed method is identical to a slightly modified version of the DAF approach. For the purposes of validation, numerical results using the proposed method are compared with available exact solutions and numerical simulation for some non-linear oscillators, and for the systems considered excellent results over the main body and tails of the distribution are obtained. The accuracy and efficiency of the method are compared to Langley's finite element method (FEM). The results indicate that the proposed approach is more accurate than the FEM when using the same number of nodal/grid points, and uses coarser meshes to obtain similar (or higher) levels of accuracy.

2. THE FPK EQUATION

In order to apply the FPK equation it is convenient to express the equations of motion in state-space notation as follows:

$$\dot{\mathbf{x}} = \mathbf{g}(\mathbf{x}) + \mathbf{A}\mathbf{w}, \tag{1}$$

where $\mathbf{x}$ is an n-dimensional vector containing the state-space variables of the system, $\mathbf{A}$ is a square matrix (assumed here to be constant), $\mathbf{w}$ is a vector of uncorrelated Gaussian white-noise processes, each having a spectral density of unity, and $\mathbf{g}(\mathbf{x})$ is a general vector function of the variables $\mathbf{x}$. For equations of motion of the form of equation (1), the vector process $\mathbf{x}$ constitutes a Markov process and the joint probability density function (j.p.d.f.) of the stationary response satisfies the stationary FPK equation as follows:

$$\sum_{i=1}^{n} \frac{\partial}{\partial x_i}[g_i(\mathbf{x})p(\mathbf{x})] - \frac{1}{2}\sum_{i=1}^{n}\sum_{j=1}^{n} B_{ij}\frac{\partial^2 p(\mathbf{x})}{\partial x_i \partial x_j} = 0, \tag{2}$$

where B_{ij} is the ijth element of the matrix $\mathbf{B}$ given by $\mathbf{B} = 2\pi\mathbf{A}\mathbf{A}^{\mathrm{T}}$. In addition to satisfying equation (2), the j.p.d.f. must also satisfy the normalization condition as well as the boundary condition that $p(\mathbf{x})$ tends to zero as each of the state-space variables tends to infinity.

In the following, a numerical solution of equation (2) is sought by using a weighted residual approach with Shannon wavelets as shape functions.

3. WEIGHTED RESIDUAL APPROACH AND THE SHANNON WAVELET

Using the weighted residual approach, solutions to the FPK equation are sought by multiplying equation (2) by a weighting function $W(\mathbf{x})$ and numerically solving the resulting equation for the j.p.d.f. Following this procedure, the equation to be solved is given by

$$\int W(\mathbf{x})\left(\sum_{i=1}^{n} \frac{\partial}{\partial x_i}[g_i(\mathbf{x})p(\mathbf{x})] - \frac{1}{2}\sum_{i=1}^{n}\sum_{j=1}^{n} B_{ij}\frac{\partial^2 p(\mathbf{x})}{\partial x_i \partial x_j}\right)\mathrm{d}\mathbf{x} = 0, \tag{3}$$

where all integrations extend over the entire domain $(-\infty, \infty)$. In order to solve equation (3) it is usually assumed that the j.p.d.f. can be expressed as a sum of shape functions, the amplitudes of which are determined by evaluating equation (3) for a number of weight functions. Examples of this approach, as applied to the stationary FPK equation, are given in Bhandari and Sherrer [4] and Langley [6]. Bhandari and Sherrer used weighted Hermite polynomials as shape functions, while Langley used linear shape functions between nodal values, i.e., the finite element method (FEM). In the latter formulation, it was necessary to reduce equation (3) to the weak form of the equations since the second term appearing in equation (3) involves second order derivatives and the shape functions are linear [6]. In the proposed method, no advantage is gained by adopting the weak form of the equations, so there is no need to consider the weak form of the equations here.

Before considering the proposed method it is beneficial to note that although, in principle, any shape function can be used in the weighted residual approach, it is beneficial to use shape functions which are orthogonal. This minimizes the coupling between shape functions and has the added benefit of making the resulting equations relatively sparse in

nature. It may be noted that the Gaussian-weighted Hermite polynomials used in Sherrer's WRM are orthogonal, while the linear shape functions used in the FEM are, strictly speaking, not orthogonal. However, given that the latter shape functions are local in nature, existing over only a finite region of the response domain, they possess some properties similar to those of spatially orthogonal functions.

The weight functions adopted in the proposed method are Shannon wavelets. When using these functions it is necessary to discretize the state-space variables representing the response domain into a number of uniformly spaced grid points. Assuming that the x_ith state-space variable takes a minimum value of x_{imin} and a maximum value of x_{imax}, x_{ij}, the jth grid point for the x_ith variable, is defined as

$$x_{ij} = x_{imin} + (j-1)\Delta_i, \tag{4}$$

where $j = 1, 2, \ldots, N_i$ and Δ_i is the uniform grid spacing for the x_ith variable given by $\Delta_i = (x_{imax} - x_{imin})/(N_i - 1)$.

Using these grid points, the shape functions used is defined as follows:

$$W_{k_1 k_2 \cdots k_n}(\mathbf{x}) = \prod_{m=1}^{n} w(x_m - x_{mk_m}), \tag{5}$$

where $k_l = 1, 2, \ldots, N_l$ and

$$w(x_i - x_{ij}) = \frac{\sin\left(\dfrac{\pi}{\Delta_i}(x_i - x_{ij})\right)}{\dfrac{\pi}{\Delta_i}(x_i - x_{ij})}. \tag{6}$$

In equation (5) different shape functions are obtained by considering different combinations of $k_1, k_2, \ldots, k_n$. Thus, by considering all possible combinations, equation (3) generates $N_1 N_2 \ldots N_n$ separate equations.

The shape function $w(x_i - x_{ij})$ is commonly known as the Shannon wavelet [21], but it is also known in the literature as the sinc function or Whittaker's cardinal function [22]. The main properties of the Shannon wavelet are listed below:

(i) *Sampling function.* The Shannon wavelet acts as a sampling (interpolating) function, i.e.,

$$w(x_i - x_j) = \delta_{ij}, \tag{7}$$

where x_i and x_j are uniformly spaced grid points and δ_{ij} is the Kronecker delta. Thus, when $i = j$ the Shannon wavelet takes a value of unity, whilst on *all* other grid points it takes a value of zero.

The terminology sampling function derives from its use in signal processing applications, where it is used to reconstruct band-limited signals from knowledge of the original signal at equally spaced intervals. Since the reconstructed signal is identical to the original signal at the sample points, it is also known as an interpolating function; this latter terminology will be used here. This property is useful in the proposed method and the DAF approach described in section 4, as it ensures that the resulting matrix equations are relatively sparse in nature.

(ii) *Spatial orthogonality.* The Shannon wavelet is spatially orthogonal, such that

$$\int_{-\infty}^{\infty} w(x - x_i) w(x - x_j)\, \mathrm{d}x = \delta_{ij}, \tag{8}$$

where δ_{ij} is the Kronecker delta. This property is particularly important here as it helps to minimize the coupling between shape functions in the proposed method.

(iii) *Dirac delta function.* Using the properties of the Fourier transform of the Shannon wavelet [23], it can be shown that the following equation is satisfied:

$$\int_{-\infty}^{\infty} w(x - x_i) \frac{\mathrm{d}^n w(x - x_j)}{\mathrm{d}x^n} \mathrm{d}x = \frac{\mathrm{d}^n w(x_i - x_j)}{\mathrm{d}x^n}. \tag{9}$$

This result is valid for $n = 0, 1, 2, 3, \ldots$ and indicates that the Shannon wavelet acts as a Dirac delta function when operating on itself and its derivatives. When $n = 0$, it may be seen that equation (9) reduces to $w(x_i - x_j)$. By making use of property (i), that $w(x_i - x_j) = \delta_{ij}$, it follows that this result is consistent with property (ii). Further, by using equation (9) it can be deduced that, for the particular class of function $h(x)$ such that

$$h(x) = \sum_i h(x_i) w(x - x_i), \tag{10}$$

the following result holds:

$$\int_{-\infty}^{\infty} w(x - x_i) \frac{\mathrm{d}^n h(x)}{\mathrm{d}x^n} \mathrm{d}x = \frac{\mathrm{d}^n h(x_i - x_j)}{\mathrm{d}x^n} \tag{11}$$

where $n = 0, 1, 2, \ldots$.

In the following, properties (i)–(iii) of the Shannon wavelet are used within the proposed weighted residual approach to determine a numerical solution procedure for the stationary FPK equation.

In order to apply the weighted residual approach, as stated earlier, it is necessary to express the j.p.d.f. as a weighted sum of shape functions. This is achieved here by letting

$$p(\mathbf{x}) = \sum_{l_1=1}^{N_1} \sum_{l_2=1}^{N_2} \cdots \sum_{l_n=1}^{N_n} \left(\prod_{m=1}^{n} w(x_m - x_{ml_m}) \right) p(x_{1l_1}, x_{2l_2}, \ldots, x_{nl_n}), \tag{12}$$

where it may be noted that the interpolating nature of the Shannon wavelet ensures that the amplitude of the shape function is identical to the value of the j.p.d.f. on the grid points. Thus, the proposed representation is similar to the FEM in that the j.p.d.f. is expressed in terms of its nodal values.

To complete the weighted residual approach, equation (12) is substituted into equation (3) and then the appropriate integrations are performed. For the purposes of presentation, it is convenient to apply this procedure to the second term of equation (3), before considering the first term.

Let us consider the second term of equation (3). Using equations (7–12) it may be shown that

$$\int W_{k_1 k_2 \ldots k_n}(\mathbf{x}) \frac{\partial^2 p(\mathbf{x})}{\partial x_i \partial x_j} \mathrm{d}\mathbf{x} = \begin{cases} \displaystyle\sum_{l_i=1}^{N_i} \sum_{l_j=1}^{N_j} \frac{\partial w(x_{ik_i} - x_{il_i})}{\partial x_i} \frac{\partial w(x_{jk_j} - x_{jl_j})}{\partial x_j} p(x_{1k_1}, x_{2k_2}, \ldots, x_{il_i}, \ldots, x_{jl_j}, \ldots, x_{nk_n}), & j \neq i, \\ \displaystyle\sum_{l_i=1}^{N_i} \frac{\partial^2 w(x_{ik_i} - x_{il_i})}{\partial x_i^2} p(x_{1k_1}, x_{2k_2}, \ldots, x_{il_i}, \ldots, x_{nk_n}) & j = i, \end{cases} \tag{13}$$

where it may be noted that the terms involving w can be evaluated analytically using equation (6).

Let us now consider the first term appearing in equation (3). Examination of equation (3) reveals that the integrals appearing in the first term involve the general vector function $g(\mathbf{x})$. To avoid having to perform these integrals, which it may not be possible to do analytically, $p(\mathbf{x})g(\mathbf{x})$ can be expressed as a sum of shape functions, such that

$$p(\mathbf{x})\mathbf{g}(\mathbf{x}) = \sum_{j_1=1}^{N_1}\sum_{j_2=1}^{N_2}\cdots\sum_{j_n=1}^{N_n}\left(\prod_{m=1}^{n} w(x_m - x_{mj_m})\right)p(x_{1j_1}, x_{2j_2}, \ldots, x_{nj_n})\mathbf{g}(x_{1j_1}, x_{2j_2}, \ldots, x_{nj_n}). \tag{14}$$

Given that $p(\mathbf{x})$ was expressed as a sum of shape function in equation (12), equation (14) corresponds to replacing $g(\mathbf{x})$ by some approximation, $g_{approx}(\mathbf{x})$ (say). Substituting equation (12) into the left-hand side of equation (14) and rearranging, it is easy to show that

$$g_{approx}(\mathbf{x}) = \frac{\sum_{j_1=1}^{N_1}\sum_{j_2=1}^{N_2}\cdots\sum_{j_n=1}^{N_n}(\prod_{m=1}^{n} w(x_m - x_{mj_m}))p(x_{1j_1}, x_{2j_2}, \ldots, x_{nj_n})\mathbf{g}(x_{1j_1}, x_{2j_2}, \ldots, x_{nj_n})}{\sum_{l_1=1}^{N_1}\sum_{l_2=1}^{N_2}\cdots\sum_{l_n=1}^{N_n}(\prod_{m=1}^{n} w(x_m - x_{ml_m}))p(x_{1l_1}, x_{2l_2}, \ldots, x_{nl_n})} \tag{15}$$

It is difficult in general to quantify the differences between $g_{approx}(\mathbf{x})$ and $g(\mathbf{x})$ from this equation. However, it may be deduced (using the interpolating nature of the Shannon wavelet) that $g_{approx}(\mathbf{x})$ is identical to $g(\mathbf{x})$ on the grid points. Thus, provided that the spacing between grid points is sufficiently small, it is expected that $g_{approx}(\mathbf{x})$ will be a good approximation to $g(\mathbf{x})$. The validity of this argument has been confirmed numerically for a variety of systems including those considered in the numerical examples section later. However, it should be noted that the greatest discrepancies between $g_{approx}(\mathbf{x})$ and $g(\mathbf{x})$ occur near the edges of the mesh used and outside of the region covered by the mesh.

Using equations (7–11) and (14) it may be shown that

$$\int W_{k_1k_2\ldots k_n}(\mathbf{x})\frac{\partial}{\partial x_i}[g_i(\mathbf{x})p(\mathbf{x})]\,\mathrm{d}\mathbf{x} = \sum_{l_i=1}^{N_i}\frac{\partial w(x_{ik_i} - x_{il_i})}{\partial x_i}g(x_{1k_1}, x_{2k_2}, \ldots, x_{il_i}, \ldots, x_{nk_n})p(x_{1k_1}, x_{2k_2}, \ldots, x_{il_i}, \ldots, x_{nk_n}). \tag{16}$$

As with equation (13), the terms involving w can be evaluated analytically using equation (6), while the vector non-linearity g will be known on the grid points.

Substituting equations (13) and (16) into equation (3), and considering all possible combinations of $k_1, k_2, \ldots, k_n$, a total of $N_1N_2\ldots N_n$ equations in terms of the $N_1N_2\ldots N_n$ unknown values of the j.p.d.f. on the uniform mesh of grid points is obtained. These equations can be expressed in vector–matrix notation as follows:

$$\mathbf{Ap} = \mathbf{0}, \tag{17}$$

where vector $\mathbf{p}$ contains the values of the j.p.d.f. on the mesh of grid points. For one-dimensional systems matrix $\mathbf{A}$ is a fully populated matrix, while for two- and higher-dimensional systems the population of matrix $\mathbf{A}$ is very much dependent upon the B_{ij} terms appearing in the second term of equation (2). For the systems considered in the numerical examples section, the matrices are relatively sparse. The reason for this is that in these cases

the FPK equation does not include any mixed derivative terms (because there is only one excitation source) and the Shannon wavelet is an interpolating function. However, the presence of mixed derivative terms will tend to increase the population of the matrix. Non-trivial solutions to equation (17) are obtained by applying the normalization condition and then solving numerically using standard techniques (see, e.g., reference [6]).

Having developed a weighted residual approach for the numerical solution of the stationary FPK equation using Shannon wavelets as basis functions, the following section considers the relationship of this method to the distributed approximating functional approach.

4. DISTRIBUTED APPROXIMATING FUNCTIONAL APPROACH

The basic concept behind the distributed approximating functional (DAF) approach is to represent the j.p.d.f. by the multi-dimensional convolution integral:

$$p(\mathbf{x}) = \int_{-\infty}^{\infty} \delta(\mathbf{x} - \mathbf{y}) p(\mathbf{y})\, \mathrm{d}\mathbf{y}, \tag{18}$$

where $\mathrm{d}\mathbf{y} = \mathrm{d}y_1 \mathrm{d}y_2 \ldots \mathrm{d}y_n$,

$$\delta(\mathbf{x} - \mathbf{y}) = \prod_{i=1}^{n} \delta(x_i - y_i), \tag{19}$$

and δ is the Dirac delta function.

In the DAF approach an approximate representation of the Dirac delta function is used and the integration appearing in equation (18) is discretized using a finite uniform grid. Following this procedure, the j.p.d.f. is approximated as follows:

$$p(\mathbf{x}) = \sum_{l_1=1}^{N_1} \sum_{l_2=1}^{N_2} \cdots \sum_{l_n=1}^{N_n} \left(\prod_{m=1}^{n} \delta(x_m - x_{ml_m}) \Delta_m \right) p(x_{1l_1}, x_{2l_2}, \ldots, x_{nl_n}), \tag{20}$$

where $\delta(x)$ is an approximate representation of the Dirac delta function and Δ_m denotes the grid spacing along the mth state-space variable. All other notation used is in accordance with that defined in section 3. In equation (18) the response domain $\mathbf{x}$ is identical to $\mathbf{y}$. For this reason, the discretized values of the $\mathbf{y}$ domain have been replaced by discretized values of the $\mathbf{x}$ domain, where the uniform grid points used are identical to those defined in equation (4). Finally, it is worthwhile noting that equation (20) has the same form as equation (12) and that they would be identical if $\delta(x)\Delta = w(x)$.

Provided that a suitable approximate representation of the Dirac delta function is available, equation (20) can be differentiated analytically to determine the derivatives of $p(\mathbf{x})$ in terms of the values of $p(\mathbf{x})$ on the grid points. Furthermore, since the Dirac delta function $\delta(x)$ peakes at $x = 0$ and tends to zero as $|x| \to \infty$, it may be deduced that the largest contributions to the derivatives will arise from those grid values closest to the point considered.

In the following, equation (20) is used as a means for determining a numerical solution to the stationary FPK equation. In the standard DAF approach it is necessary to substitute equation (20) into equation (2) and then evaluate the unknown values of the j.p.d.f. on the grid points by setting the residual to zero when $\mathbf{x}$ lies on a grid point. This is equivalent to using a series of Dirac delta functions centred on each grid point to weight the residual, and

is identical to applying a collocation method. Following this procedure, it can be seen from equation (2) that it is necessary to differentiate $p(\mathbf{x})$ w.r.t. x_i, where $i = 1, 2, \ldots, n$. Provided that the approximation to the Dirac delta function used is a continuous, twice differentiable function, this can be achieved easily by differentiating equation (20). This is an important feature of the DAF approach, and, in principle, it can be used to determine derivatives of arbitrary order, making it a powerful computational tool for solving certain ordinary and partial differential equations.

In certain respects the DAF approach is similar to the traditional PDE orthogonal collocation method (OCM) [24]. Using this method, $p(\mathbf{x})$ would be expressed as a weighted sum of orthogonal shape functions, the amplitudes of which would be determined by setting the residual to zero at the so-called "collocation" points. One of the most obvious differences between this method and the DAF approach is that the DAF shape functions are chosen to be approximations to the Dirac delta function which are not necessarily orthogonal. Another difference is that the DAF approach yields amplitudes of the shape functions which are effectively the value of $p(\mathbf{x})$ at the grid points, while the OCM yields amplitudes which must be manipulated further to determine $p(\mathbf{x})$. Furthermore, in the application described above, the DAF shape functions are chosen so that their equivalent collocation points lie on a uniform grid, whilst those of the OCM would be the roots of the highest orthogonal function used, which would tend *not* be uniformly spaced.

Here a slightly modified version of the DAF approach is presented which, with a suitable choice of Dirac delta function, will be shown to be identical to the weighted residual approach proposed in section 3. In this formulation, the modification corresponds to expressing $p(\mathbf{x})g(\mathbf{x})$, which appears in the first term of equation (2), as follows:

$$p(\mathbf{x})\mathbf{g}(\mathbf{x}) = \int_{-\infty}^{\infty} \delta(\mathbf{x} - \mathbf{y}) p(\mathbf{y})\mathbf{g}(\mathbf{y})\, \mathrm{d}\mathbf{y}. \tag{21}$$

In discretized form (i.e., as a sum of Dirac delta functions) this is approximated as

$$p(\mathbf{x})\mathbf{g}(\mathbf{x}) = \sum_{l_1=1}^{N_1} \sum_{l_2=1}^{N_2} \cdots \sum_{l_n=1}^{N_n} \left(\prod_{m=1}^{n} \delta(x_m - x_{ml_m}) \Delta_m \right) p(x_{1l_1}, x_{2l_2}, \ldots, x_{nl_n}) \mathbf{g}(x_{1l_1}, x_{2l_2}, \ldots, x_{nl_n}). \tag{22}$$

In principle, it is perfectly valid to adopt equation (21). However, since an approximate representation of the Dirac delta function is used in equations (20) and (22), a degree of approximation regarding the form of $g(\mathbf{x})$ is introduced when adopting equation (22). This approximation is similar to that introduced in equation (14), and can be shown to approximate $\mathbf{g}(\mathbf{x})$ by $\mathbf{g}_{approx}(\mathbf{x})$ (say) where

$$\mathbf{g}_{approx}(\mathbf{x}) = \frac{\sum_{j_1=1}^{N_1} \sum_{j_2=1}^{N_2} \cdots \sum_{j_n=1}^{N_n} \left(\prod_{m=1}^{n} \delta(x_m - x_{mj_m}) \Delta_m \right) p(x_{1j_1}, x_{2j_2}, \ldots, x_{nj_n}) \mathbf{g}(x_{1j_1}, x_{2j_2}, \ldots, x_{nj_n})}{\sum_{l_1=1}^{N_1} \sum_{l_2=1}^{N_2} \cdots \sum_{l_n=1}^{N_n} \left(\prod_{m=1}^{n} \delta(x_m - x_{ml_m}) \Delta_m \right) p(x_{1l_1}, x_{2l_2}, \ldots, x_{nl_n})}. \tag{23}$$

The accuracy of this approximation is very much dependent upon the approximation used to represent the Dirac delta function. For example, if the representation of the Dirac delta function used is an interpolating (sampling) function, such that

$$\delta(x_i - x_j)\Delta = \delta_{ij}, \tag{24}$$

where δ_{ij} is the Kronecker delta, then $\mathbf{g}_{approx}(\mathbf{x})$ will be identical to $\mathbf{g}(\mathbf{x})$ on the grid points. However, if a non-interpolating function is used, such as that obtained by expanding the Dirac delta function as a weighted Hermite polynomial [16], then this will not be the case.

Using equation (22) it may be shown that:

$$\frac{\partial}{\partial x_i}[\mathbf{g}_i(\mathbf{x})p(\mathbf{x})] = \sum_{l_1=1}^{N_1}\sum_{l_2=1}^{N_2}\cdots\sum_{l_n=1}^{N_n}\left(\prod_{\substack{m=1\\m\neq i}}^{n}\delta(x_m - x_{ml_m})\Delta_m\right) \times\frac{\partial}{\partial x_i}[\delta(x_i - x_{il_i})]p(x_{1l_1}, x_{2l_2}, \ldots, x_{nl_n})\mathbf{g}(x_{1l_1}, x_{2l_2}, \ldots, x_{nl_n})\Delta_i. \tag{25}$$

Following the standard DAF approach, the second term in equation (2) is evaluated using equation (20) to give

$$\frac{\partial^2 p(\mathbf{x})}{\partial x_i \partial x_j} = \begin{cases} \displaystyle\sum_{l_1=1}^{N_1}\sum_{l_2=1}^{N_2}\cdots\sum_{l_n=1}^{N_n}\left(\prod_{\substack{m=1\\m\neq i\\m\neq j}}^{n}\delta(x_m - x_{ml_m})\Delta_m\right)\frac{\partial}{\partial x_i}[\delta(x_i - x_{il_i})] \\ \qquad\times\dfrac{\partial}{\partial x_j}[\delta(x_j - x_{jl_j})]p(x_{1l_1}, x_{2l_2}, \ldots, x_{nl_n})\Delta_i\Delta_j \quad j\neq i, \\ \displaystyle\sum_{l_1=1}^{N_1}\sum_{l_2=1}^{N_2}\cdots\sum_{l_n=1}^{N_n}\left(\prod_{\substack{m=1\\m\neq i}}^{n}\delta(x_m - x_{ml_m})\Delta_m\right) \\ \qquad\times\dfrac{\partial^2}{\partial x_i^2}[\delta(x_i - x_{il_i})]p(x_{1l_1}, x_{2l_2}, \ldots, x_{nl_n})\Delta_i \quad j = i. \end{cases} \tag{26}$$

To complete the formulation of the DAF approach, equations (25) and (26) are substituted into equation (2) and the unknown values of the j.p.d.f. on the grid points evaluated by setting the residual to zero when $\mathbf{x}$ lies on a grid point. This is equivalent to using the Dirac delta function to weight the residual, and is identical to applying a collocation method. In general, this procedure results in $N_1N_2\ldots N_n$ equations in terms of the $N_1N_2\ldots N_n$ unknown values of the j.p.d.f. on the uniform mesh of grid points, and the equations can be expressed in vector–matrix notation in a similar manner to equation (17).

For a practical implementation it is necessary to select an approximate representation of the Dirac delta function which can be used in equations (25) and (26). A variety of possibilities exist for this purpose. Before considering these it is worthwhile considering the formal definition of the Dirac delta function, which is [25]

$$\delta(x) = \begin{cases} \infty & \text{if } x = 0, \\ 0 & \text{otherwise} \end{cases} \tag{27}$$

and

$$\int_{-\infty}^{\infty}\delta(x)\,\mathrm{d}x = 1. \tag{28}$$

It should be noted that it is not practical to use the definition afforded by equation (27). However, some representations exist which do satisfy equation (28). These include: (i) the pulse function; (ii) a weighted Hermite polynomial representation; and (iii) the Shannon wavelet. Each of these is considered in what follows.

(i) *Pulse function.* This is the simplest possible representation of the Dirac delta function and is given by

$$\delta(x) = \begin{cases} \dfrac{1}{\Delta}, & -\dfrac{\Delta}{2} \leqslant x \leqslant \dfrac{\Delta}{2}, \\ 0 & \text{otherwise.} \end{cases} \tag{29}$$

This representation is not well-suited to the DAF approach since it is neither continuous nor differentiable. However, by using difference formulae to approximate the derivatives it is possible to use equation (29) in equations (25) and (26). Following this procedure it may be shown that the finite difference (FD) method is obtained. The main advantage of this formulation is that the resulting matrices are extremely sparse. However, in practice a large number of grid points are required to obtain accurate estimates of the derivatives and hence the dimensions of the resulting matrix are prohibitively large, giving rise to excessively large computing times.

(ii) *Weighted Hermite polynomials.* It is possible to express the Dirac delta function as a weighted series of Hermite polynomials, such that [26]

$$\delta(x) = \frac{1}{\sqrt{2\pi}\sigma} \exp\left(-\frac{x^2}{2\sigma^2} \right) \sum_{k=0}^{\infty} \mathrm{H}_{2k}(0) \mathrm{H}_{2k}\left(\frac{x}{\sigma} \right), \tag{30}$$

where H_j is the jth Hermite polynomial, and

$$H_{2k}(0) = \begin{cases} 1, & k = 0, \\ \dfrac{(-1)^k (2k-1)!}{2^{k-1}(k-1)!(2k)!}, & k = 1, 2, 3, \ldots \end{cases}. \tag{31}$$

This representation is well-suited to the DAF approach and is known in the literature as the Hermite DAF [16]. In contrast to the pulse function, this representation yields a continuous, differentiable representation of the Dirac delta function. A practical implementation of the method requires that the infinite series appearing in equation (30) be truncated and a value of σ chosen. Some success with this representation for solving the stationary FPK equation of a non-linear oscillator subjected to white noise has been reported recently by McWilliam [26]. However, the main disadvantage of this representation is that it is *not* an interpolating function, and consequently always yields matrix equations that are fully populated. For low order systems (i.e., 1-D and 2-D systems) this does not provide much difficulty. However, for higher order systems it is likely that the computer storage requirements will become excessive, leading to excessively long computer run times.

(iii) *Shannon wavelet*. This representation is based upon approximating the Dirac delta function as a band-limited function and is given by

$$\delta(x) = \frac{\sin(\pi x/\Delta)}{\pi x}, \tag{32}$$

where Δ is the uniform spacing between grid points. This representation is well-suited to the DAF approach as it is continuous and differentiable. It also has the advantage over the Hermite DAF in that it is an interpolating function, producing matrix equations that have the potential to be relatively sparse. In addition to satisfying equation (28), it may be noted that the Shannon wavelet also possesses certain orthogonal properties (see equation (8)). The orthogonal properties are a fundamental characteristic of the Dirac delta function and arise as a direct result of equation (27). A perceived disadvantage of equation (32) is that it tends to zero quite slowly as $|x| \to \infty$ (i.e., decays as $1/x$). A direct consequence of this is that when calculating the derivatives of the j.p.d.f. using equations (25) and (26) a large number of the nodal values will contribute significantly. It is for this reason that Hoffman *et al.* [20] have recently suggested using the Shannon–Gabor wavelet in the DAF approach, in which the Dirac delta function is expressed as

$$\delta(x) = \frac{\sin(\pi x/\Delta)}{\pi x} \exp\left(-\frac{x^2}{2\sigma^2}\right), \tag{33}$$

where σ is the standard deviation of the Gabor transform (or Gaussian window function). Of course, as $\sigma \to \infty$, equation (33) tends to the Shannon wavelet. This representation has the advantage that for finite σ it tends to zero much more quickly than the Shannon wavelet as $|x| \to \infty$. In some ways this improves the approximation to a Dirac delta function. A consequence of this it that it ensures that derivatives at any one point are more dependent on the neighbouring nodal values than on the nodal values further away from the point considered. However, the presence of the Gaussian window in equation (33) destroys the orthogonal properties possessed by the Shannon wavelet, effectively worsening the approximation to a Dirac delta function.

In the following, the Shannon wavelet representation of the Dirac delta function is adopted, and it is shown that this representation ensures that the (modified) DAF approach is identical to the weighted residual approach described in section 3.

Replacing $\delta(x - x_i)\Delta$ by $w(x - x_i)$ in equations (25) and (26), where $w(x - x_i)$ is given by equation (6), and letting

$$\mathbf{x} = (x_{1k_1}, x_{2k_2}, \ldots, x_{nk_n}), \tag{34}$$

gives

$$\frac{\partial}{\partial x_i}[g_i(\mathbf{x})p(\mathbf{x})]\bigg|_{\mathbf{x}=(x_{1k_1}, x_{2k_2}, \ldots, x_{nk_n})}$$

$$= \sum_{l_1=1}^{N_1} \sum_{l_2=1}^{N_2} \cdots \sum_{l_n=1}^{N_n} \left(\prod_{\substack{m=1 \\ m \neq i}}^{n} w(x_m - x_{ml_m}) \right) \frac{\partial}{\partial x_i}[w(x_i - x_{il_i})]\, p(x_{1l_1}, x_{2l_2}, \ldots, x_{nl_n}) \mathbf{g}(x_{1l_1}, x_{2l_2}, \ldots, x_{nl_n}), \tag{35}$$

and

$$\left.\frac{\partial^2 p(\mathbf{x})}{\partial x_i \partial x_j}\right|_{\mathbf{x}=(x_1 k_1, x_2 k_2 \cdots x_n k_n)}$$

$$= \begin{cases} \displaystyle\sum_{l_1=1}^{N_1}\sum_{l_2=1}^{N_2}\cdots\sum_{l_n=1}^{N_n}\left(\prod_{\substack{m=1\\ m\neq i\\ m\neq j}}^{n} w(x_{mk_m}-x_{ml_m})\Delta_m\right)\frac{\partial}{\partial x_i}[w(x_{ik_m}-x_{il_i})] \\ \qquad \times\dfrac{\partial}{\partial x_j}[w(x_{jk_i}-x_{jl_j})]p(x_{1l_1},x_{2l_2},\ldots,x_{nl_n}), \quad j\neq i, \\ \displaystyle\sum_{l_1=1}^{N_1}\sum_{l_2=1}^{N_2}\cdots\sum_{l_n=1}^{N_n}\left(\prod_{\substack{m=1\\ m\neq i}}^{n} w(x_{mk_m}-x_{ml_m})\right) \\ \qquad \times\dfrac{\partial^2}{\partial x_i^2}[w(x_{ik_i}-x_{il_i})]\,p(x_{1l_1},x_{2l_2},\ldots,x_{nl_n}) \quad j=i. \end{cases} \tag{36}$$

Using the fact that the Shannon wavelet is an interpolating function (equation (7)) in equations (35) and (36) and comparing the resulting expressions with equations (16) and (13) respectively, it may be deduced that

$$\left.\frac{\partial}{\partial x_i}[g_i(\mathbf{x})p(\mathbf{x})]\right|_{\mathbf{x}=(x_{1k_1},x_{2k_2},\ldots,x_{nk_n})} = \int W_{k_1k_2..k_n}(\mathbf{x})\frac{\partial}{\partial x_i}[g_i(\mathbf{x})p(\mathbf{x})]\,\mathrm{d}\mathbf{x}, \tag{37}$$

and

$$\left.\frac{\partial^2 p(\mathbf{x})}{\partial x_i \partial x_j}\right|_{\mathbf{x}=(x_{1k_1},x_{2k_2},\ldots,x_{nk_n})} = \int W_{k_1k_2\ldots k_n}(\mathbf{x})\frac{\partial^2 p(\mathbf{x})}{\partial x_i \partial x_j}\,\mathrm{d}\mathbf{x}. \tag{38}$$

The terms appearing on the left-hand side of equations (37) and (38) correspond to those obtained using the modified DAF approach using Shannon wavelets to represent the Dirac delta function. From these equations it may be seen that they are equivalent to those derived using the weighted residual approach described in section 3, where Shannon wavelets are used as shape functions. Thus it may be concluded that the weighted residual approach described in section 3 is identical to a modified DAF approach (equations (16) and (13)) when Shannon wavelets are used to represent the Dirac delta function. This result may be proved more efficiently by noting that equations (20) and (22) ensure that $p(\mathbf{x})\mathbf{g}(\mathbf{x})$ and $p(\mathbf{x})$ belong to the particular class of functions (equation (10)) for which equation (11) holds. Consequently, equations (37) and (38) follow immediately.

5. NUMERICAL EXAMPLES

This section considers the accuracy and efficiency of the proposed method for a number of non-linear, single-degree-freedom systems with varying amounts of non-linearity. In all cases the j.p.d.f.'s are calculated and then integrated to give the marginal displacement and velocity p.d.f.'s which are more convenient to view. The marginal distributions are plotted on

normalized axes, where the displacement and velocity are expressed in terms of the number of standard deviations from the mean and the normalized p.d.f. value is obtained by multiplying the marginal p.d.f. by the r.m.s. response. In all cases they are plotted on linear and logarithmic scales so that the accuracy of the proposed method over the main body and "tails" can be examined. The results plotted on log-scales are especially important if the results are to be used in extreme response calculations. Comparisons are made with an equivalent Gaussian distribution to give an indication of the non-Gaussian nature of the response and the exact analytic solution. Comparisons are also made with results obtained using Langley's finite element method (FEM) [6] so that the accuracy of the proposed method can be assessed compared to the FEM. These comparisons are made qualitatively by comparing the marginal densities on the same graphical scale and quantitatively by using two measures of error for the marginal displacement p.d.f. The first measure of error e_1 is given by

$$e_1 = \sqrt{\frac{1}{N}\sum_{i=1}^{N} (p(x_i) - p_{exact}(x_i))^2}, \tag{39}$$

where $N(= N_1 = N_2)$ defines the number of grid points used to discretize the response domain, $p(x_i)$ is the calculated displacement p.d.f., and $p_{exact}(x_i)$ is the exact displacement p.d.f. Equation (39) provides a general measure of the accuracy of the solution over the main body of the distribution and was used by Langtangen [7] to investigate the accuracy of the FEM. The second measure of error e_2 provides a measure of the accuracy of the solution at the "tails" of the distribution and is given by

$$e_2 = \sqrt{\frac{1}{N}\sum_{i=1}^{N} \left(\frac{p(x_i) - p_{exact}(x_i)}{p_{exact}(x_i)}\right)^2}. \tag{40}$$

Unlike the path integral method, the proposed method and the FEM are not guaranteed to produce p.d.f.'s that are always positive. When calculating response distributions using the FEM and the proposed method, negative values tend to occur at the edges of the response domain where assumptions are made regarding the form of the j.p.d.f. outside of the response domain considered. Within the FEM this is usually taken into account by selecting response domains for analysis that are much larger than the area of interest [6], confining the least-accurate results to areas that are of little practical interest. This procedure will be adopted here for both the proposed method and the FEM. As a consequence, the measure of error given by equation (40) is restricted here to values of the marginal distribution $p(x_i)$ that have values greater than 10^{-6}. This method for assessing the error at the tails was first adopted by Langtangen [7].

The efficiency of the solution procedure is assessed by comparing the CPU times (in s) taken to execute the numerical procedure with those obtained using the FEM. The CPU times it takes to generate and solve equation (17) on a UNIX Workstation are compared. To provide an unbiased comparison NAG routine F04AAF is used in all cases to solve the resulting matrix equations. This routine uses a standard storage routine, which ensures that computer storage space is proportional to mesh size. Use of this routine will undoubtedly influence the performance of the techniques considered, since the sparse nature of coefficient matrix **A** appearing in equation (17) (both for the proposed method and the FEM) is not made use of. By using the same routine, both methods are subjected to the same constraint of having to solve fully populated systems of equations. Given that the FEM yields coefficient matrices that are less populated than the proposed method, this will hinder the performance of the FEM more than the proposed method. The degree to which the FEM is hindered will

TABLE 1

Comparison of CPU times (in s) to generate the coefficient matrix and solve the resulting equations for the proposed method and FEM for different mesh sizes

Mesh size	Proposed method		Finite element method	
$(N_1 \times N_2)$	Generate matrix	Solve equations	Generate matrix	Solve equations
21×21	0·04	2·4	0·12	0·11
31×31	0·18	15·5	0·29	0·72
41×41	0·57	109	0·52	4
51×51	1·4	524	0·79	11
61×61	3·9	1496	1·15	29

be system dependent, since the space requirement depends on the scaling and structure of the coefficient matrix [9]. For the systems considered here, the same systematic node numbering is used for the proposed method and FEM. However, it is acknowledged that reductions in the CPU time may be achieved by using sparse matrix routines, as indicated by the results presented by Dunne and Ghanbari [9]. Furthermore, it is obvious that as the order of the system increases, the storage requirement will increase quickly if fully populated matrices are used. In these situations, sparse routines could be adopted. However, an alternative approach may be to generate the transient response starting from suitable initial conditions until the stationary response is reached.

The sparse nature of the coefficient matrix for the systems considered ensures that the CPU times are (to a good approximation) dependent only on the number of nodal values used. Consequently, the resulting CPU times are approximately system independent. Table 1 summarizes the CPU times for all of the numerical examples considered. (Note that although respective times in seconds are stated, it is the relative magnitudes of these that are important.) In each case two values are given: the first corresponds to the time taken to generate the coefficient matrix, while the second corresponds to the time taken to solve the resulting set of equations. It may be seen from Table 1 that the proposed method is more numerically intense than the FEM to both generate and solve the coefficient matrix for identical mesh sizes. However, in what follows it will be shown that the proposed method yields results of superior accuracy to the FEM using much coarser meshes. Thus, provided that the (total) CPU time using the proposed method with a coarser mesh is less than that obtained using the FEM with a finer mesh, it will be shown that the proposed method can be more efficient than the FEM.

5.1. LINEAR OSCILLATOR

The equation of motion to be considered here is given by

$$\begin{aligned} \dot{x}_1 &= x_2, \\ \dot{x}_2 &= -x_2 - x_1 + f, \end{aligned} \tag{41}$$

where f is a zero mean, Gaussian, white-noise excitation with a constant spectral density value $S_0 = 1/\pi$. The stationary response statistics are calculated using a mesh of points and

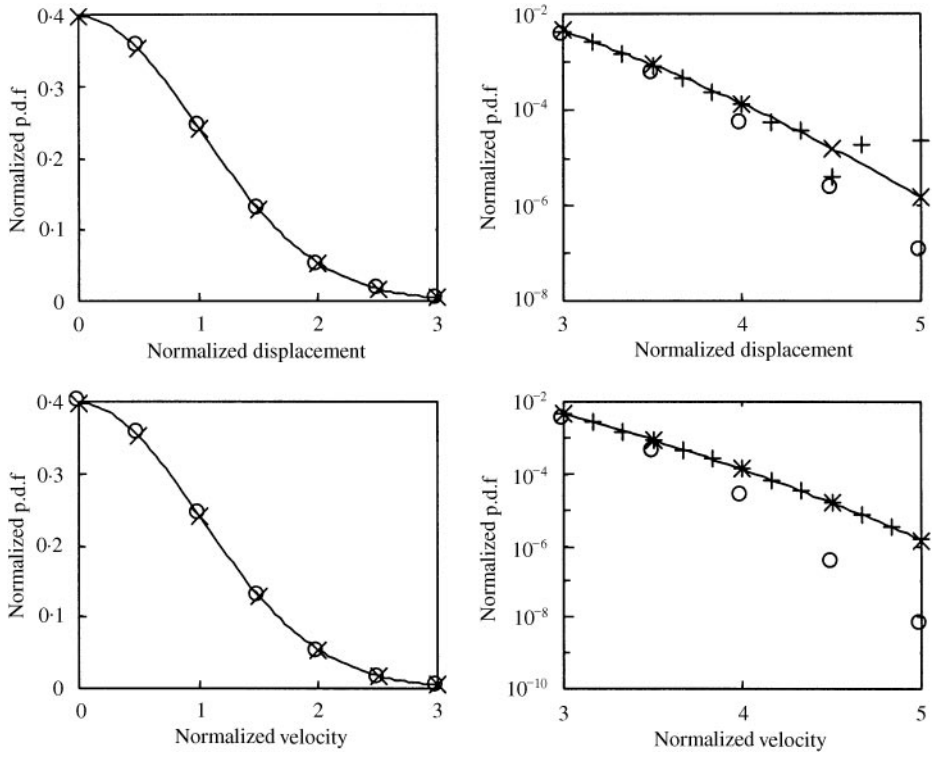

Figure 1. Response statistics of a linear oscillator: ——, exact analytical solution, ×, proposed method ($N_1 = N_2 = 21$); ○, FEM ($N_1 = N_2 = 21$); +, FEM ($N_1 = N_2 = 61$).

response domain such that $N_1 = N_2 = 21$ and $-5\sigma_1 \leqslant x_1 \leqslant 5\sigma_1$ and $-5\sigma_2 \leqslant x_2 \leqslant 5\sigma_2$, where σ_1 and σ_2 are the standard deviations of the displacement (x_1) and velocity (x_2) response respectively. The results for this situation are shown in Figure 1. There it may be seen that the proposed method yields excellent agreement with the exact result over the main body of the distribution and the "tails". The FEM gives results that are in good agreement over the main body, while the agreement at the tails deteriorates. For this reason the number of grid points was increased so that $N_1 = N_2 = 61$. For clarity of presentation, these results are shown only on the logarithmic axes in Figure 1. However, even with this increase, the FEM still deviates visibly from the exact result at the tails of the displacement p.d.f. Taking into account the CPU times presented in Table 1, it may be seen that, for the results shown, the proposed method with $N_1 = N_2 = 21$ provides a more efficient numerical procedure than the FEM with $N_1 = N_2 = 61$ for the system considered.

In this example, the displacement and velocity are statistically independent, and the displacement and velocity distributions are identical. However, it can be seen in Figure 1 that the FEM produces results for the displacement and velocity distributions that are not the same. The reason for this can be explained by noting that the governing FPK equation involves derivatives up to second order w.r.t. velocity and only first order w.r.t. displacement. Thus, even though the j.p.d.f. is symmetric, the matrix appearing in equation (17) is altered when the displacement and velocity are interchanged. As a consequence the calculated j.p.d.f. is not guaranteed to be symmetric and the marginal distributions are not guaranteed to be the same. The fact that this discrepancy is quite distinct in the FEM results even when an increased number of grid points is present, highlights the approximate nature of the FEM.

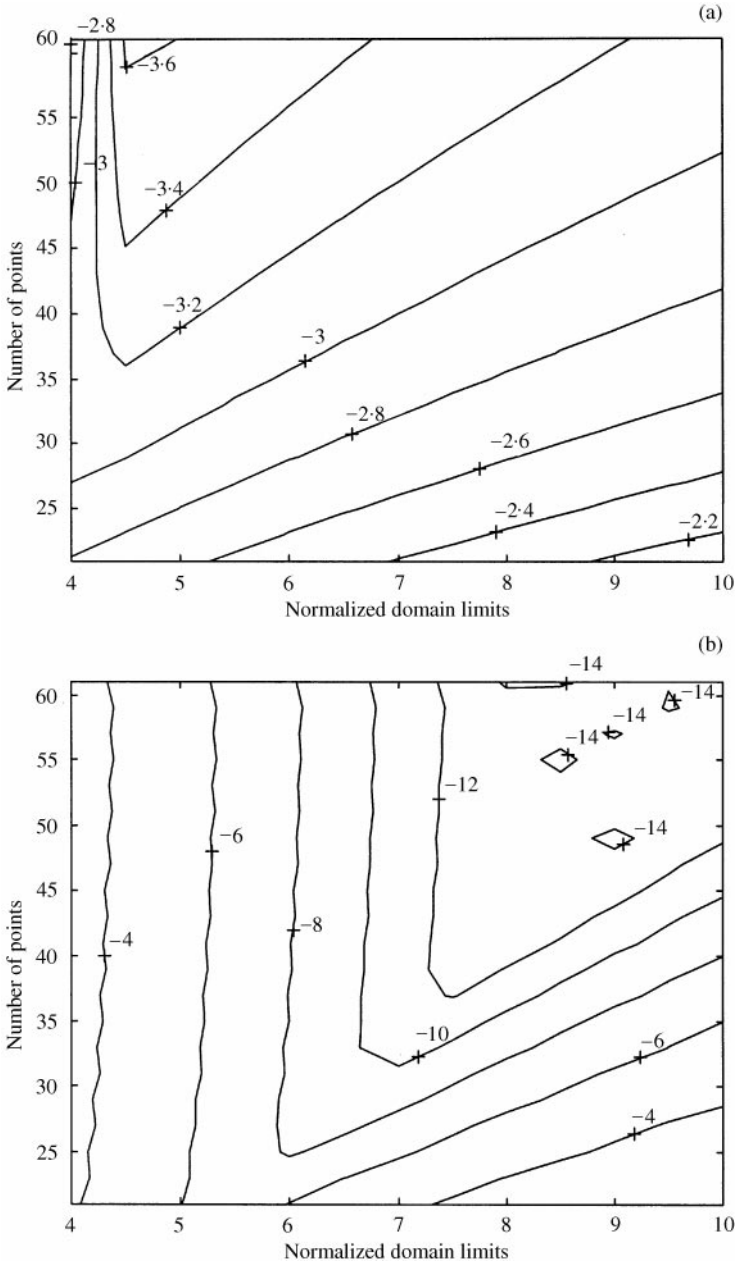

Figure 2. Contour plots of $\log_{10}(e_1)$ for different numbers of grid points N ($= N_1 = N_2$) and domain limits for a linear oscillator: (a) FEM; (b) proposed method.

In contrast, the proposed method produces results for the displacement and velocity distributions that, on the graphical scale used, are identical. This provides an indication of the superior accuracy provided by the proposed method compared to the FEM.

Figures 2(a) and 2(b) show logarithmic contour plots of the error e_1 for different mesh sizes and normalized domain limits using the FEM and proposed method respectively. In this

example, the normalized domain limits correspond to the number of standard deviations on either side of the mean used to represent the displacement–velocity response domain. For example, a normalized domain limit of 6 corresponds to a mesh such that, $-6\sigma_1 \leqslant x_1 \leqslant 6\sigma_1$ and $-6\sigma_2 \leqslant x_2 \leqslant 6\sigma_2$. Figure 2(a) shows that when using the FEM with a constant domain, an increase in the number of grid points increases the accuracy of the solution. This is because as the grid spacing decreases, the linear shape functions used within the FEM provide a better approximation to the j.p.d.f. The same is true when the number of grid points is kept constant and the size of the response domain is decreased. However, when the normalized response domain is less than 5, the errors tend to increase. The reason for this is that for very small response domains it is not possible to satisfy the normalization condition. Thus, it may be concluded for the FEM that the finer the mesh of points, the more accurate the solution becomes provided that the normalization condition is satisfied. In contrast, Figure 2(b) indicates that the proposed method yields most accurate results when *both* the domain limits and mesh size are increased. This may be explained by recalling that Shannon wavelets are used as shape functions in the proposed method. Given that these shape functions decay quite slowly, it is beneficial to increase the size of the response domain to ensure that the nodal values at the edges of the mesh take the smallest values possible. Further, a corresponding increase in the number of grid points will increase the resolution by increasing the Nyquist frequency.

Comparing the results shown in Figures 2(a) and 2(b) it can be seen that the error obtained using the FEM for each given value of mesh size and domain limits is an order of magnitude larger than that obtained using the proposed method. Consequently, accurate results may be obtained using a relatively large range of response domain sizes and grid mesh sizes, suggesting that the proposed method is not sensitive to the choice of these parameters. Furthermore, it can be seen that for any given domain limit the proposed method produces results that are more accurate than the FEM using fewer grid points.

The results presented in Figure 2 are calculated using a measure of error that is applicable to the main body of the distribution. To check the validity of the above conclusions over the tails of the distribution it is necessary to consider the measure of error defined by equation (40). Results obtained using this equation are shown in Figures 3(a) and 3(b) which show logarithmic contour plots of error e_2 for different mesh sizes and normalized domain limits using the FEM and proposed method respectively. These results are in qualitative agreement with those shown in Figure 2 and provide evidence that the conclusions presented earlier for error e_1 are similarly valid for error e_2. Given the similarities between the errors e_1 and e_2 and the fact that error e_1 provides more readable contour plots than e_2, later discussions will be limited to e_1 only.

5.2. DUFFING OSCILLATOR

The equation of motion to be considered here is given by

$$\dot{x}_1 = x_2$$

$$\dot{x}_2 = -x_2 - x_1 - \tfrac{1}{2}x_1^3 + f, \tag{42}$$

where f is a zero mean, Gaussian, white-noise excitation with a constant spectral density value $S_0 = 1/\pi$. Equation (42) represents a reasonably non-linear system that has mono-modal displacement and velocity p.d.f.'s. The stationary marginal distributions for this case are shown in Figure 4, where the displacement and velocity domains are taken to be

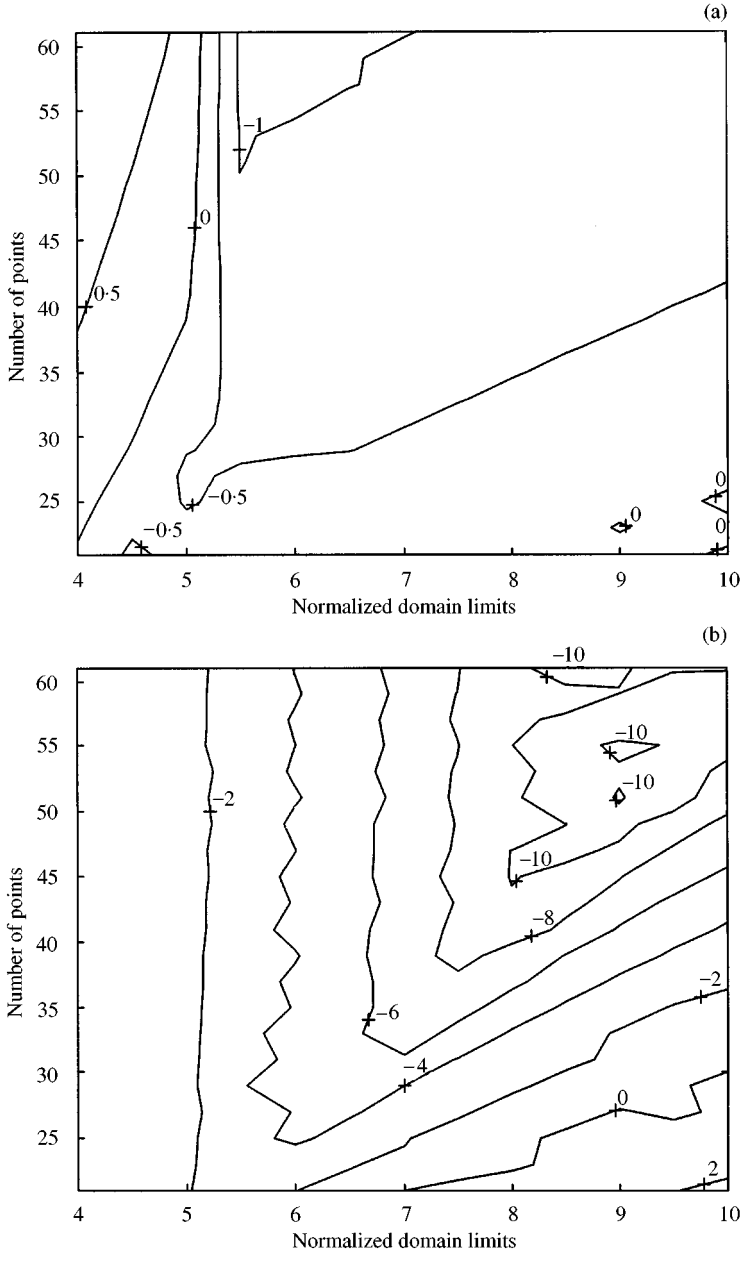

Figure 3. Contour plots of $\log_{10}(e_2)$ for different numbers of grid points N ($= N_1 = N_2$) and domain limits for a linear oscillator: (a) FEM; (b) proposed method.

$-4\sigma_1 \leqslant x_1 \leqslant 4\sigma_1$ and $-5\sigma_2 \leqslant x_2 \leqslant 5\sigma_2$, and the grid points such that $N_1 = N_2 = 31$. With the exception of the extreme "tails" of the distribution, where the solution deviates from the exact, the proposed method is seen to be in excellent agreement with the exact result with a reasonably coarse mesh. In contrast, the FEM yields poor results over the tails of the displacement and velocity p.d.f.'s. To overcome these inaccuracies, an increased number of grid points are used to represent the response domain ($N_1 = N_2 = 61$), and the results are

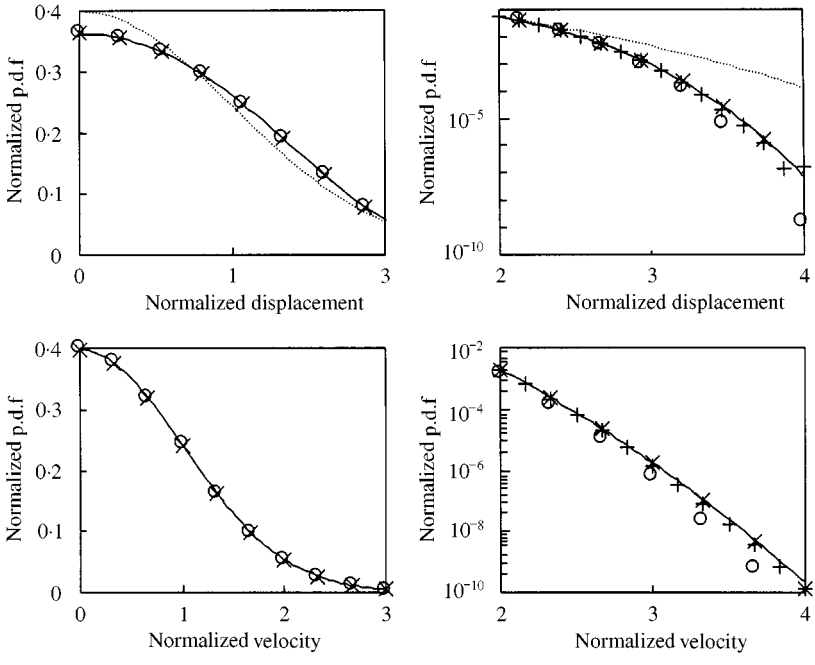

Figure 4. Response statistics of a Duffing oscillator: ——, exact analytical solution, ×, proposed method ($N_1 = N_2 = 31$); ○, FEM ($N_1 = N_2 = 31$), +, FEM ($N_1 = N_2 = 61$); ----, equivalent Gaussian distribution (displacement only).

shown on the logarithmic axes in Figure 4. There it can be seen that the FEM now gives better agreement over the main body of the distributions, but still underestimates the tails. From a practical perspective it may be argued that the accuracy obtained using the FEM is acceptable. From Table 1 it can be seen that the total CPU time associated with the proposed method with $N_1 = N_2 = 31$ is less than that associated with the FEM with $N_1 = N_2 = 61$. Thus, for the results presented it can be deduced that the proposed method is more efficient than the FEM.

Figures 5(a) and 5(b) shows logarithmic contour plots of error e_1 using different mesh sizes and normalized domain limits for the FEM and the proposed method respectively. There the normalized domain limits correspond to the number of standard deviations on either side of the mean used to represent the displacement response domain, and the number of standard deviations divided by 1·25 used to represent the velocity domain. For example, a normalized domain limit of 5 corresponds to a mesh such that: $-5\sigma_1 \leqslant x_1 \leqslant 5\sigma_1$ and $-6{\cdot}25\sigma_2 \leqslant x_2 \leqslant 6{\cdot}25\sigma_2$. In Figure 5 it can be seen that similar conclusions can be drawn for the Duffing oscillator as for the linear oscillator, suggesting that the proposed method is intrinsically more accurate than the FEM. Although not shown, similar findings have been observed for the e_2 error, indicating that the proposed method yields accurate results for the displacement p.d.f. for practical values of interest, that is values of probability density down to 10^{-6}.

Naess and Johnsen [11] and Yu *et al.* [13] have used the path integral method produce accurate results to probability density levels of 10^{-10}. Figure 6 shows that by increasing the number of grid points such that $N_1 = N_2 = 61$, and increasing the domain limits to $-8{\cdot}125\sigma_1 \leqslant x_1 \leqslant 8{\cdot}125\sigma_1$ and $-6{\cdot}5\sigma_2 \leqslant x_2 \leqslant 6{\cdot}5\sigma_2$, the proposed method yields

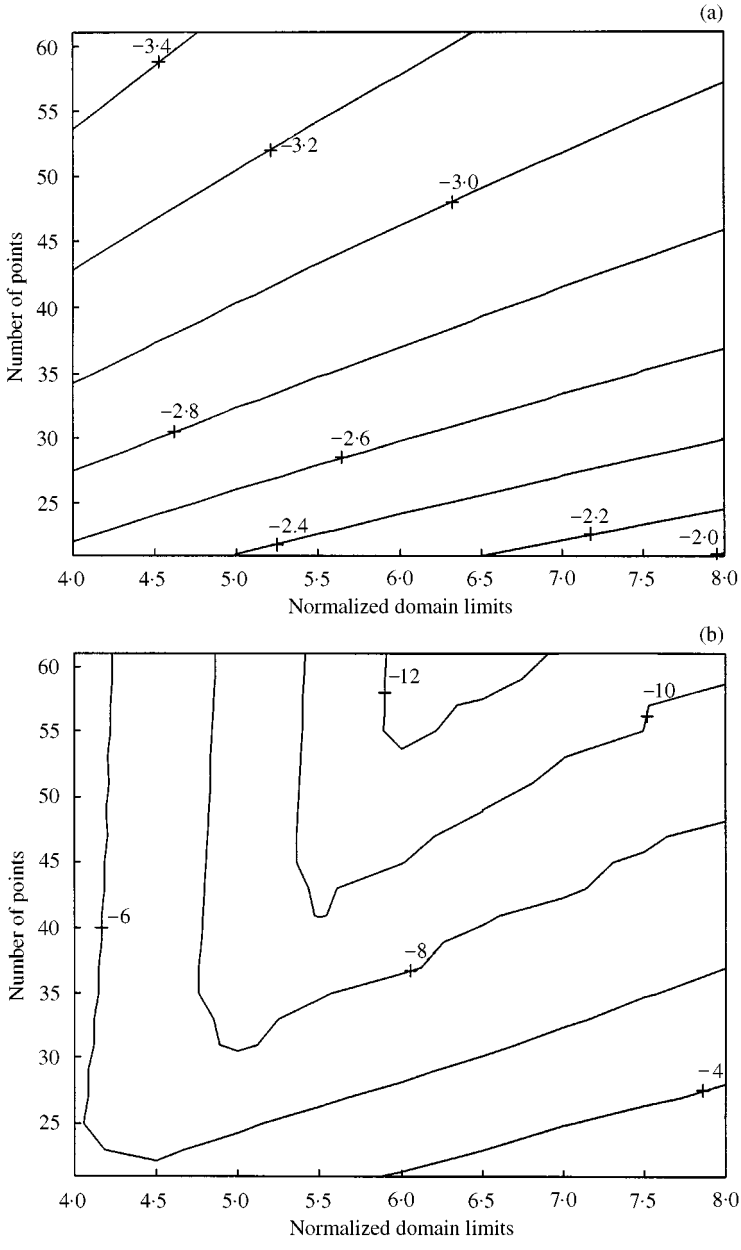

Figure 5. Contour plots of $\log_{10}(e_1)$ for different numbers of grid points N ($= N_1 = N_2$) and domain limits for a Duffing oscillator: (a) FEM; (b) proposed method.

accurate results down to very low probability levels. It may be noted, however, that these results are in poor agreement with the exact distribution at the very tails of the distribution. This is indicated in Figure 6 by the presence, on logarithmic axes, of a distinctive "shallow" region at the extreme of the response domain. This region exists because outside of the response domain considered, the assumed form for the j.p.d.f. ensures that the distribution decays at the same (slow) rate as the Shannon wavelet (i.e., as $1/x$). Similar inaccuracies occur

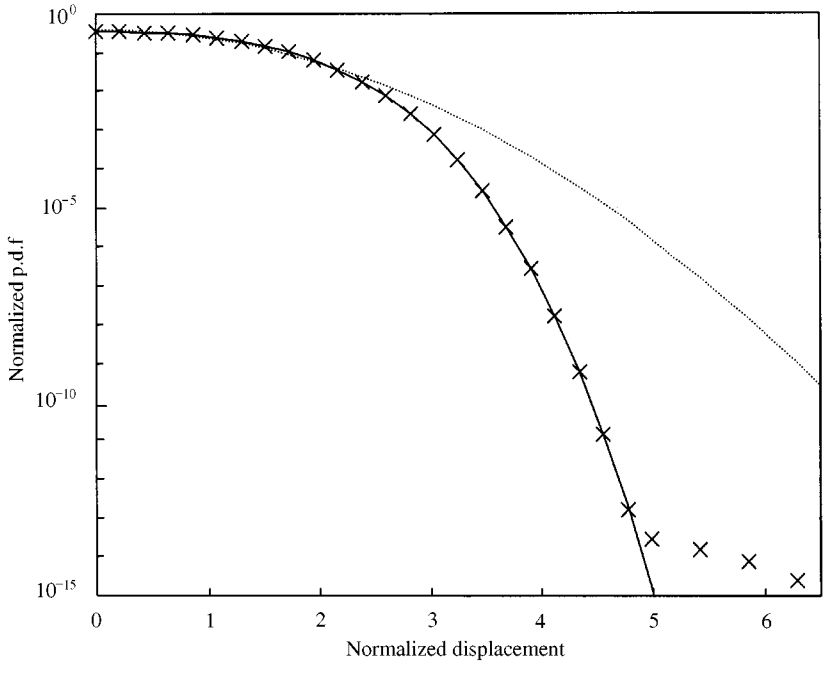

Figure 6. Displacement statistics of a Duffing oscillator: ——, exact solution, ×, proposed method ($N_1 = N_2 = 61$); ----, equivalent Gaussian distribution.

when the FEM is used. As noted earlier, it is advisable to select the limits of the response domain so that the less-accurate results, which occur at the tails, lie outside the region of interest. However, it is interesting to note in this case that the calculated results remain in close agreement with the exact result up to a critical point beyond which the gradient suddenly increases. Given that the critical point is easily identifiable it suggests that for those situations when the exact solution is not known the transition from regions of high accuracy to low accuracy will be easily identifiable because of the sudden increase in the gradient of the log p.d.f. Although not shown here, similar trends have been observed for other systems by the authors.

5.3. OSCILLATOR WITH ENERGY-DEPENDENT DAMPING

The equation of motion to be considered here is given by (see reference [15])

$$\dot{x}_1 = x_2,$$

$$\dot{x}_2 = -\beta x_2 - \alpha(x_1^2 + x_2^2)x_2 - x_1 + f, \tag{43}$$

where $f(t)$ is a zero mean, Gaussian, white-noise excitation with a constant spectral value $S_0 = 1/\pi$. For the case considered let $\beta = -0{\cdot}5$, $\alpha = 0{\cdot}125$. The stationary response statistics for this case are calculated using a response domain such that $-3\sigma_1 \leqslant x_1 \leqslant 3\sigma_1$ and $-3\sigma_2 \leqslant x_2 \leqslant 3\sigma_2$, and a grid mesh of points such that $N_1 = N_2 = 41$. The marginal distributions are identical in this case and the results obtained for this situation are shown in Figure 7. From these results it can be seen that the proposed method gives excellent

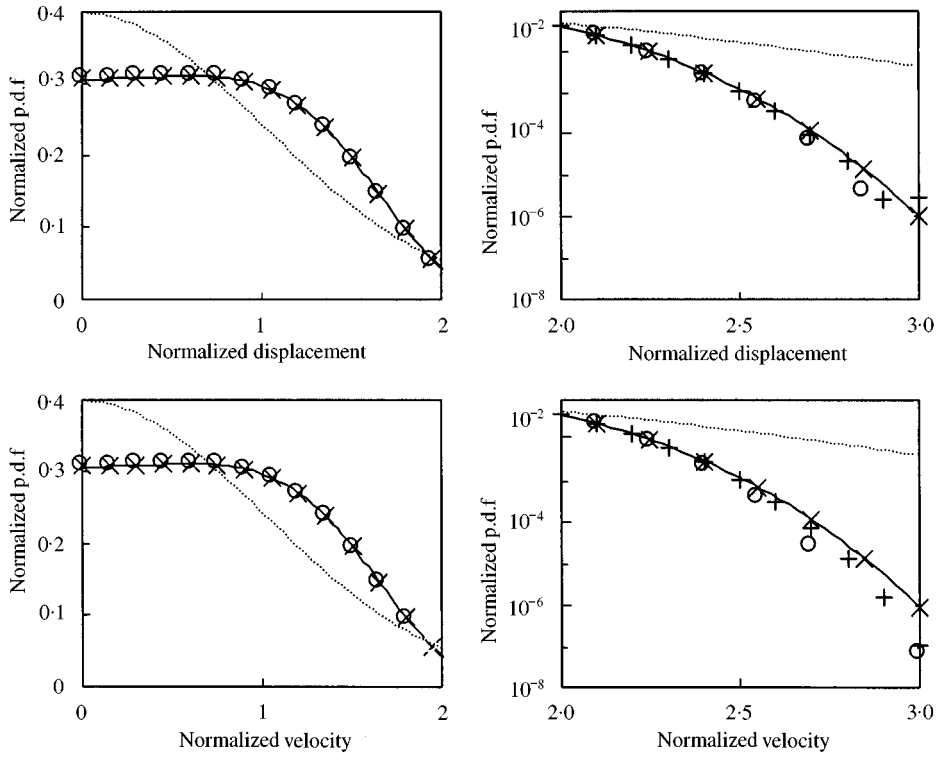

Figure 7. Response statistics of an oscillator with energy dependent damping (see Example 3): ——, exact solution; ×, proposed method ($N_1 = N_2 = 41$); ○, FEM ($N_1 = N_2 = 41$), +, FEM ($N_1 = N_2 = 61$), ----, equivalent Gaussian distribution.

agreement with the exact result, both over the main body of the curve and up to the tails. The FEM results underestimate the "tails" of the p.d.f.'s and yield some negative values at the tails. For this reason the number of grid points for the FEM was increased to $N_1 = N_2 = 61$. As with the linear oscillator, the approximate nature of the FEM is highlighted by the fact that the results for the displacement and velocity p.d.f.'s are visibly different when they should be identical. It should also be noted that the proposed method provides superior accuracy compared to the FEM, using fewer elements to achieve higher levels of accuracy. This conclusion is further justified in Figure 8, which shows logarithmic plots for error e_1 with different mesh sizes and normalized domain limits. There the normalized domain limits are identical to those defined for the linear oscillator, and it can be seen for most values of domain limit that the proposed method yields results to a higher level of accuracy than the FEM, using a coarser mesh.

Despite the greater accuracy achieved using the proposed method it is pertinent to recall the results shown in Figure 7. There it was observed that the proposed method required a mesh size such that $N_1 = N_2 = 41$ (with $-3\sigma_1 \leqslant x_1 \leqslant 3\sigma_1$ and $-3\sigma_2 \leqslant x_2 \leqslant 3\sigma_2$) to achieve accurate results on the graphical scale used, while the FEM required $N_1 = N_2 = 61$. A comparison of the CPU times taken to achieve these results indicates that the FEM provides a *more efficient* solution procedure than the proposed method, provided that one is willing to accept the accuracy indicated in Figure 7. Thus, although Figure 8 indicates that the proposed method is inherently more accurate than the proposed method, it is not necessarily more efficient, provided one is willing to accept a certain degree of inaccuracy.

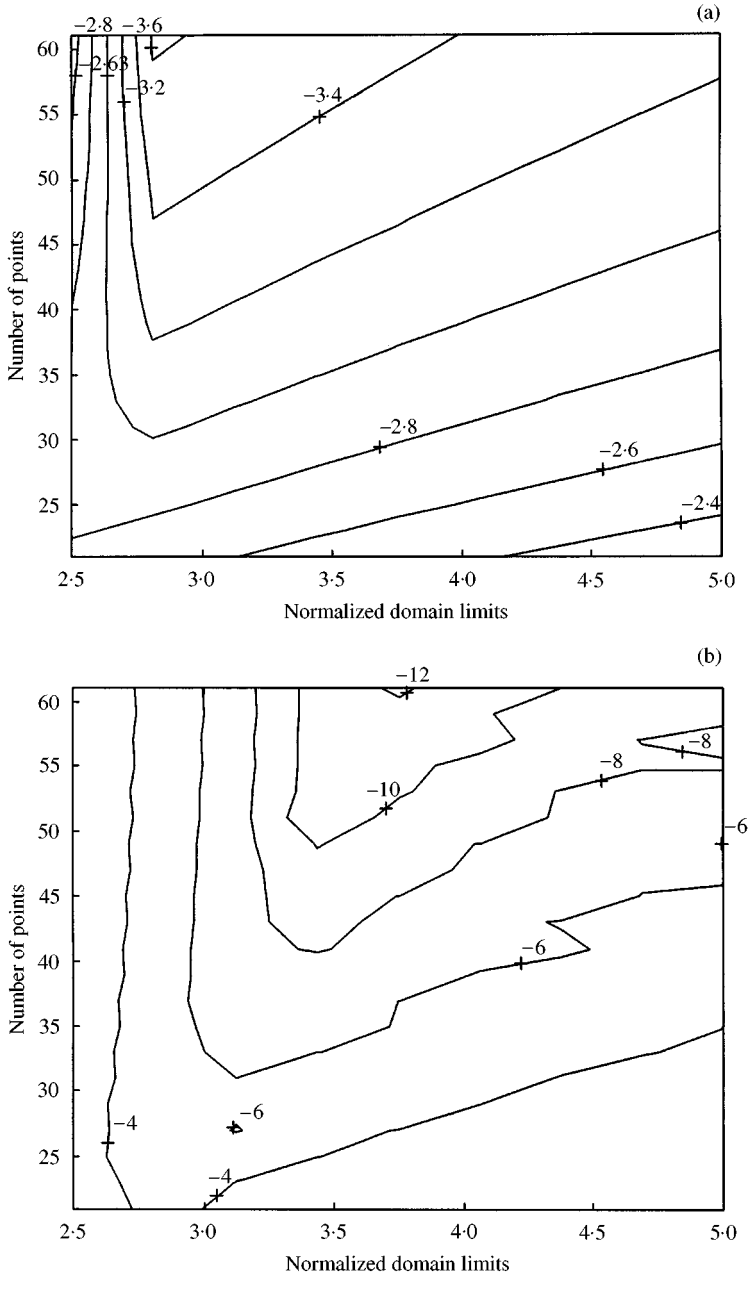

Figure 8. Contour plots of $\log_{10}(e_1)$ for different numbers of grid points N ($= N_1 = N_2$) and domain limits for an oscillator with energy dependent damping: (a) FEM; (b) proposed method.

5.4. SHIP ROLL PROBLEM

The equation of motion to be considered here is given by (see references [3, 6])

$$\dot{x}_1 = x_2,$$
$$\dot{x}_2 = -ax_2 - bx_2|x_2| - x_1 + x_1^3 + f, \tag{44}$$

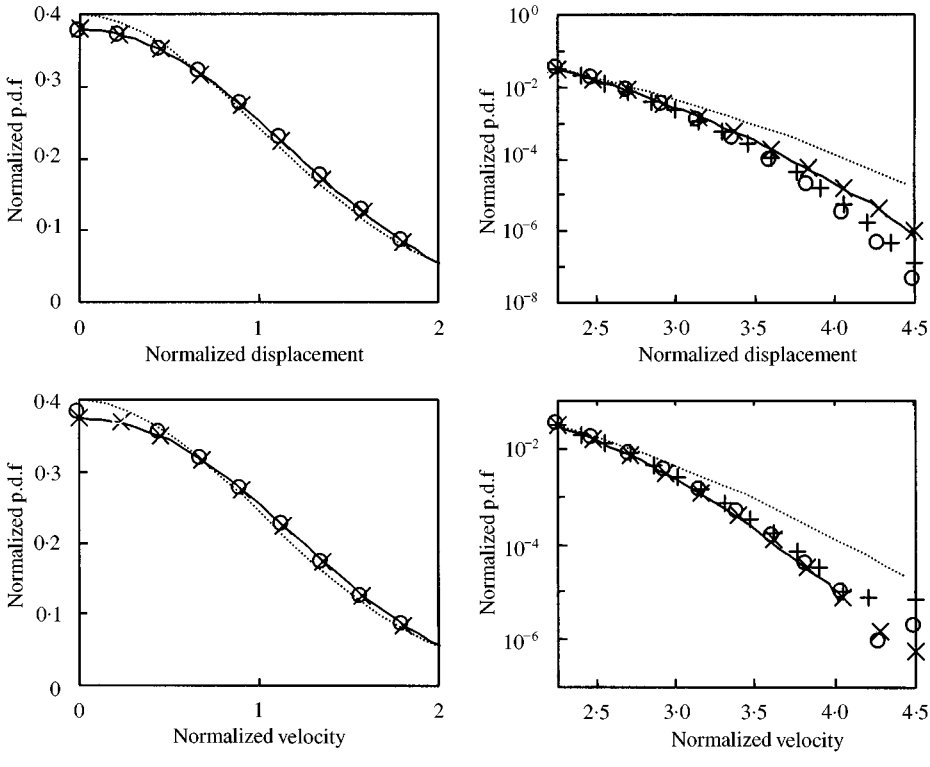

Figure 9. Response statistics for the ship roll problem (see Example 4): ——, simulation; ×, proposed method ($N_1 = N_2 = 41$); ○, FEM ($N_1 = N_2 = 41$); +, FEM ($N_1 = N_2 = 61$); ----, equivalent Gaussian distribution.

where $f(t)$ is a zero mean, Gaussian, white-noise excitation with a constant spectral value $S_0 = 4{\cdot}476 \times 10^{-4}$. A highly non-linear case is considered [6] in which $a = 0{\cdot}1$ and $b = 1{\cdot}0$. The stationary response statistics are calculated using a response domain such that $-4{\cdot}5\sigma_1 \leqslant x_1 \leqslant 4{\cdot}5\sigma_1$ and $-4{\cdot}5\sigma_2 \leqslant x_2 \leqslant 4{\cdot}5\sigma_2$, and a grid mesh of points such that $N_1 = N_2 = 41$. Unlike the previous examples, there is no *exact* analytical solution available. For this reason the results obtained are compared with numerical simulation. The numerical results are obtained by using the FFT technique to generate a time history and a fourth-order Runge–Kutta scheme to calculate the corresponding time-history for the response. The response p.d.f. is then calculated directly from the time-history for the response, where for the results presented over 25 000 h of simulation were combined to ensure that a reliable estimate of the tails of the distribution was obtained. From these simulations, the r.m.s. responses were found to be 0·0804 and 0·0795 for x_1 and x_2 respectively. The marginal distributions for the response are shown in Figure 9. From these results, it can be seen that the proposed method gives excellent agreement with simulation, both over the main body and tails. Although the FEM results are in good agreement with the velocity p.d.f., they underestimate the "tails" of the displacement p.d.f. For this reason the number of grid points for the FEM was increased to $N_1 = N_2 = 61$. These results provide the FEM with improved accuracy, but are still not as accurate as the results obtained using the proposed method. Given that no exact result exists for the system considered, it is not possible to assess the error using equations (39) and (40).

At this stage, as with the previous example, it is worthwhile considering the CPU times associated with using the proposed method for the current example. Table 1 indicates that as

the grid size increases the CPU time for the proposed method increases rapidly compared to the FEM. Thus, although the proposed method provides increased accuracy compared to the FEM, it is unlikely to provide a more efficient solution procedure unless the FEM requires many more elements than the proposed method. For the case considered here (and the previous example), this appears unlikely to be the case, and as a consequence the FEM is the more efficient solution procedure, provided that a reduced level of accuracy is acceptable. Recalling that the proposed method was observed to be more efficient for the linear and Duffing oscillators considered and noting that these examples were not as non-linear as the last two examples, it may be suggested from the results presented that the proposed method is more efficient than the FEM for reasonably non-linear systems, while for more highly non-linear systems the FEM will be more efficient.

6. CONCLUSIONS

A weighted residual approach to solving the stationary FPK equation has been presented in which Shannon wavelets have been used as shape functions. The relationship between the proposed method and the recently developed DAF approach has been considered and it was found that the weighted residual approach yields equations which are identical to those produced by a modified version of the DAF approach using Shannon wavelets to represent the Dirac delta function. In essence, the link between the two methods arises from the orthogonal properties of the Shannon wavelet and the relationship between the Shannon wavelet and the Dirac delta function. For the systems considered, it was found that the proposed method yielded results which were in excellent agreement with known exact results, both over the main body of the marginal response distributions and the "tails". Furthermore, a comparison with the finite element method indicated that the proposed method required fewer grid points to produce results of greater accuracy. Although better accuracy was achieved using the proposed method, the FEM was found to be intrinsically less numerically intensive for a comparable sized mesh due to the greater sparsity of the coefficient matrix. (Further increases in efficiency may be obtained by using sparse matrix routines, but these were not investigated here.) In some cases, this meant that *similar* degrees of accuracy could be obtained more efficiently using the FEM with a suitably large number of grid points than using the proposed method with fewer grid points. This was observed for the highly non-linear cases considered. For the less non-linear systems considered the proposed method yielded both more accurate and efficient results than the FEM. Thus, it is suggested that the proposed method is preferable to the FEM for systems containing moderate non-linearities.

A future publication will consider the application of the proposed method to determine the mean up-crossing rate and response statistics of higher order systems.

REFERENCES

1. Y. K. LIN 1967 *Probabilistic Theory of Structural Dynamics*. New York: McGraw-Hill.
2. Y. K. LIN and G. Q. CAI 1995 *Probabilistic Structural Dynamics: Advanced Theory and Applications*. Singapore: McGraw-Hill.
3. J. B. ROBERTS 1982 *Journal of Ship Research* **26**, 229–245. A stochastic theory for nonlinear ship rolling in irregular seas.
4. R. G. BHANDARI and R. E. SHERRER 1968 *Journal of Mechanical Engineering Science*, **10**, 168–174. Random vibrations in discrete non-linear dynamic systems.
5. Y. K. WEN 1975 *Proceedings of the ASCE Journal of the Engineering Mechanics Division* **101**, 389–401. Approximate method for non-linear random vibration.

6. R. S. LANGLEY 1985 *Journal of Sound and Vibration* **101**, 41–54. A finite element method for the statistics of non-linear random vibration.
7. H. P. LANGTANGEN 1991 *Reliability Probabilistic Engineering Mechanics* **6**, 33–48. A general numerical solution method for Fokker–Planck equations with applications to structural.
8. S. F. WOJTKIEWIZC, L. A. BERGMAN and B. F. SPENCER 1994 *AAE* 94-08, *Technical Report, Aeronautical and Astronautical Engineering Department, University of Illinois.* Robust numerical solution of the Fokker–Planck–Kolmogorov equation for two dimensional stochastic dynamics systems.
9. J. F. DUNNE and M. GHANBARI 1997 *Journal of Sound and Vibration* **206**, 697–724. Extreme-value prediction for non-linear oscillators via numerical solutions of the stationary FPK equation.
10. W. YI, S. F. WOJTKIEWIZC, L. A. BERGMAN and B. F. SPENCER 1998 *International Conference on Structural Safety and Reliability* **1–3**, 859–865. Solution of Fokker–Planck equations in higher dimensions: application of the concurrent finite element method.
11. NAESS and J. M. JOHNSEN 1993 *Probabilistic Engineering Mechanics* **8**, 91–106. Response statistics of nonlinear compliant structures by the path integral solution method.
12. A. NAESS 1997 *Probabilistic Engineering Mechanics* **12**, 257–260. IASSAR Report on computational stochastic mechanics.
13. J. S. YU, G. Q. CAI and Y. K. LIN 1997 *International Journal of Non-Linear Mechanics* **32**, 759–768. A new path integration procedure based on Gauss–Legendre scheme.
14. S. MCWILLIAM 1997 *Proceedings of the 6th International Conference on Recent Advances in structural Dynamics, ISVR, Southampton*, 1581–1596. Extreme response analysis of non-linear systems to random vibration.
15. G. MUSCOLINO, G. RICCIARDI and M. VASTA 1997 *Journal of Non-linear Mechanics* **32**, 1051–1064. Stationary and non-stationary probability density functions for non-linear oscillators.
16. D. K. HOFFMAN, N. NAYER, O. A. SARAFEDDIN and D. J. KOURI 1991 *Journal of Physical Chemistry* **95**, 8299–8305. Analytic banded approximation for the discretized free propagator.
17. D. K. HOFFMAN, G. W. WEI, D. S. ZHANG and D. J. KOURI 1997 *Physical Review E, Part B* **56**, 1197–1206. Numerical method for the non-linear Fokker–Planck equation.
18. D. S. ZHANG, G. W. WEI, D. J. KOURI and D. K. HOFFMAN 1997 *Physics of Fluids* **9**, 1853–1855. Burgers' equation with high Reynolds number.
19. D. S. ZHANG, G. W. WEI, D. J. KOURI and D. K. HOFFMAN 1998 *Chemical Physics Letters* **284**, 56–62. Lagrange distributed approximating functional method for the solution of the Schrodinger equation.
20. D. K. HOFFMAN, G. W. WEI, D. S. ZHANG and D. J. KOURI 1998 *Chemical Physics Letters* **287**, 119–224. Shannon–Gabor wavelet distributed approximating functional.
21. C. K. CHUI 1992 *An Introduction to Wavelets.* New York: Academic Press.
22. D. R. HARTREE 1958 *Numerical Analysis* 93-96. Oxford: Oxford University Press, second Edition.
23. D. E. NEWLAND 1993 *An Introduction to Random Vibrations, Spectral and Wavelet Analysis.* New York: Longman, third edition.
24. W. F. AMES 1977 *Numerical Methods for Partial differential Equations.* New York: Academic Press, second edition.
25. W. B. DAVENPORT and W. L. ROOT 1958 *An Introduction to the Theory of Random Signals and Noise.* New York: McGraw-Hill.
26. S. McWilliam in press *Proceedings of the IUTAM Symposium on Non-linearity and Stochastic Structural Dynamics* 1999, *Madras, India.* Numerical solution of the stationary FPK equation for a non-linear oscillator.